Smart Structures and Systems, *Vol. 23, No. 6 (2019) 615-626*
DOI: https://doi.org/10.12989/sss.2019.23.6.615

Performance evaluation of inerter-based damping devices for structural vibration control of stay cables

Zhiwen Huang[a], Xugang Hua[*], Zhengqing Chen[b] and Huawei Niu[c]

Key Laboratory for Wind and Bridge Engineering of Hunan Province, College of Civil Engineering, Hunan University, Hunan410082, P.R. China

(Received April 21, 2017, Revised January 12, 2019, Accepted January 25, 2019)

Abstract. Inerter-based damping devices (IBBDs), which consist of inerter, spring and viscous damper, have been extensively investigated in vehicle suspension systems and demonstrated to be more effective than the traditional control devices with spring and viscous damper only. In the present study, the control performance on cable vibration reduction was studied for four different inerter-based damping devices, namely the parallel-connected viscous mass damper (PVMD), series-connected viscous mass damper (SVMD), tuned inerter dampers (TID) and tuned viscous mass damper (TVMD). Firstly the mechanism of the ball screw inerter is introduced. Then the state-space formulation of the cable-TID system is derived as an example for the cable-IBBDs system. Based on the complex modal analysis, single-mode cable vibration control analysis is conducted for PVMD, SVMD, TID and TVMD, and their optimal parameters and the maximum attainable damping ratios of the cable/damper system are obtained for several specified damper locations and modes in combination by the Nelder-Mead simplex algorithm. Lastly, optimal design of PVMD is developed for multi-mode vibration control of cable, and the results of damping ratio analysis are validated through the forced vibration analysis in a case study by numerical simulation. The results show that all the four inerter-based damping devices significantly outperform the viscous damper for single-mode vibration control. In the case of multi-mode vibration control, PVMD can provide more damping to the first four modes of cable than the viscous damper does, and their maximum control forces under resonant frequency of harmonic forced vibration are nearly the same. The results of this study clearly demonstrate the effectiveness and advantages of PVMD in cable vibration control.

Keywords: stay cable; vibration control; inerter; damper; modal damping ratio

1. Introduction

Stay cables are susceptible to a number of dynamic problems, such as wind-induced vibration, wind-rain-induced vibration, and parametric oscillation, due to their large flexibility, relatively light mass and extremely low inherent damping (Matsumoto *et al.* 1992). In order to suppress the problematic vibrations, it is effective to improve the damping of cables by external dampers installed near the cable anchorage (Duan *et al*. 2018).

Oil damper with linear viscous damping has been extensively investigated for cable vibration control due to their simplicity and effectiveness (Xu and Yu 1998, Krenk 2000, Tabatabai and Mehrabi 2000, Main and Jones 2002). For a given installation position, only the damping coefficient needs to be designed for oil damper, but maximum attainable damping ratios of the cable-damper system may be attenuated by cable sag, cable bending stiffness, cable inclination, damper stiffness and damper support stiffness alone or in combination (Yu and Xu 1998, Fujino and Hoang 2008, Fournier and Cheng 2014). Generally, oil damper is able to provide sufficient damping for short cables, even if multi-mode cable vibrations are concerned (Wang *et al*. 2005); However, oil damper may be not effective for vibration control of long cables, since its installation position is quite close to the cable anchorage compared with the cable length.

In order to obtain much higher damping for long cables, active/semi-active cable control strategy has thus been proposed and extensively studied in the last decades. Most of the studies are based on MR damper (Ni *et al.* 2002, Duan *et al.* 2005, Liu *et al.* 2007, Or *et al.* 2008, Weber *et al.* 2009, Duan *et al.* 2019a), whose damping coefficient can be easily adjusted by changing the imposed current. The effectiveness and robustness of MR damper has been verified by many researchers (Chen *et al.* 2004, Duan *et al.* 2006, Li *et al*. 2007, Duan *et al.* 2019b). Another way to improve the control performance of dampers for long cables is to combine the viscous dampers with a negative stiffness device in parallel configuration (Weber and Boston 2011). The negative stiffness enhances the damper displacements so that the damper dissipates more energy to make the cable/damper system achieve a higher supplement modal damping (Li *et al.* 2008). The development of the truly passive negative stiffness device (PNSD) was addressed in

∗Corresponding author, Professor
E-mail: cexghua@hnu.edu.cn
[a] Postdoctoral Researcher
E-mail: zwhuang213@hnu.edu.cn
[b] Professor
E-mail: zqchen@hnu.edu.cn
[c] Professor Senior Engineer
E-mail: niuhw@hnu.edu.cn

http://www.techno-press.com/journals/sss&subpage=7
ISSN: 1738-1584 (Print), 1738-1991 (Online)

detail by Sarlis (2013) and Pasala *et al*. (2014). A few investigators have analytically and experimentally studied the performance of PNSD for structural vibration control of stay cables (Chen *et al.* 2015, Shi and Zhu 2015, Zhou and Li 2016).

The damper mass or concentrated mass at the damper location can generate a pseudo-negative stiffness, which is capable of providing more damping to the cable (Krenk and Hogsberg 2005, Duan *et al.* 2006). However, a significant mass will be required to increase sustainably the attainable modal damping ratio. On the other hand, the concept of inerter, originally invented by Smith (2002), provides a practical and viable way to take advantage of damper mass and its corresponding pseudo-negative stiffness effect. Inerter is a two-terminal mechanical device, which provides a force proportional to the relative acceleration between its two terminals. The proportionality constant, called inertance or apparent mass, has the unit of kilograms and can be a factor of several thousands larger than the actual mass of the device. The inerter can be physically realized by the rack-and-pinion mechanism or ball-screw mechanism (Chen *et al.* 2009) and is usually employed together with spring and damper to constitute the inerter-based passive network (it is called the inerter-based damping device (IBDD) in this paper)(Smith and Wang 2004). IBDD has been intensively investigated in vehicle suspensions and demonstrated to be more effective and robust than the conventional passive strut consisting of spring and damper only (Wang *et al.* 2009, Chen *et al.* 2015).

In recent years, the investigation and implementation of inerter-based damping device (IBDD) have been extended to more general vibration control systems. In the field of civil engineering, various kinds of IBDDs have also been reported, most of which are used to suppress the earthquake response of building structures (Hwang *et al.* 2007, Ikago *et al*. 2012, Takewaki *et al.* 2012, Lazar *et al*. 2014, Nakamura *et al.* 2014). The potential application of IBBD on cable vibration control has also drawn attentions in the past two years. Lazar *et al*. (2016) investigated the effectiveness of the tuned inerter dampers (TID) in suppressing the cable vibration under support excitation. The results showed that TID, with sufficiently large mass ratio, can achieve a higher vibration suppression level than viscous damper. Lu *et al.* (2017) evaluated the performance of the viscous inertial mass damper (VIMD) on cable vibration control and they found that a significant improvement of the maximum attainable damping ratio can be achieved by VIMD compared with the viscous damper. Luo *et al.* (2016) investigated the performance of three inerter-based damping devices to mitigate the fundamental mode vibration of cables. It is shown that all the three devices can provide larger damping ratio than the viscous damper does.

It is noted that in all the above studies the IBDDs are only used for single-mode cable vibration control. However, typically wind-rain-induced vibration may develop for the first several modes with natural frequency up to 3 Hz (Chen *et al.* 2004), so multi-mode vibration control is also required for the design of IBBDs. Additionally, even for the single-mode cable vibration control based on IBDD, the influence of damper location and mode number on the optimum parameters and maximum attainable damping ratio has not been clarified yet. In this study, control performances of four inerter-based damping devices for stay cables are assessed in terms of supplemental modal damping ratio. They are the parallel-connected viscous mass damper (PVMD), series-connected viscous mass damper (SVMD), tuned inerter dampers (TID) and tuned viscous mass damper (TVMD). In the first section, the mechanism of the ball screw inerter is introduced. Then the state-space formulation of the cable-IBBD system is derived and single-mode vibration control analysis was conducted for PVMD, SVMD, TID and TVMD. Their optimum parameters and the maximum attainable modal damping ratios are obtained for several specified damper locations and modes in combination by the Nelder-Mead simplex algorithm. Optimal design of PVMD is also developed for multi-mode cable vibration control, and the results of damping ratio analysis are examined through a forced vibration analysis by numerical simulation.

2. Inerter and inerter-based damping devices (IBDDs)

2.1 The mechanism of ball screw inerter

A schematic of the ball screw inerter is shown in Fig. 1 to illustrate the mass amplifying mechanism. The ball screw inerter is composed of a ball screw, a ball nut, a flywheel, an external tube and two thrust bearings. The flywheel rigidly connected to the ball nut is supported by the thrust bearings, which are installed on the external tube. When a relative motion is given between the two ends of the inerter, that is node 1 and node 2, the ball nut and the flywheel are rotated by the ball screw and they produce an inertial torque proportional to the angular acceleration of the ball nut. Due to the ball screw mechanism, the inertial torque is reconverted to an axial resisting force applied on the ball screw and transmitted to the structure through node 1 and node 2.

The rotational angle of the ball nut and flywheel is given by

$$\theta = \frac{2\pi}{L_e} u \tag{1}$$

where θ is the rotational angle of the ball nut; u is the relative displacement of the two ends of the damper; L_e is the lead of the ball screw. The inertial torque, T_f, generated by the revolving flywheel is given by

$$T_f = I_f \ddot{\theta} \tag{2}$$

where I_f and $\ddot{\theta}$ are the moment of inertia and angular acceleration of flywheel, respectively. If all the friction loss in the ball screw transmission is neglected, the axial force, F, produced by the ideal inerter is given by

$$F = \frac{2\pi}{L_e} T_f \tag{3}$$

Substituting Eqs. (1) and (2) into Eq. (3), we obtain

$$F=\left(\frac{2\pi}{L_e}\right)^2 I_f\ddot{u}=\overline{m}_e\ddot{u} \tag{4}$$

where $\overline{m}_e$ denotes the inertance or apparent mass of the inerter. If the flywheel is made in the shape of a hollow cylinder as shown in Fig. 1, its moment of inertia can be given by

$$I_f=\frac{1}{2}m_0(r_i^2+r_o^2) \tag{5}$$

where

$$m_0=\rho\pi(r_o^2-r_i^2)h \tag{6}$$

where m_0 is the mass of flywheel; r_i and r_o are the inner radius and outer radius of flywheel, respectively; h is the length of flywheel; ρ is the material density.

In order to understand the mass amplification effect of the inerter, we calculate the apparent mass of an assumed inerter for cable application. The lead of the ball screw is L_e=0.01 m, the inner radius, length and density of the flywheel is r_i=0.05 m, h=0.2 m and ρ=7850 kg/m^3, respectively. Thus the variations of the apparent mass and actual mass of the flywheel with its outer radius are shown in Fig. 2.

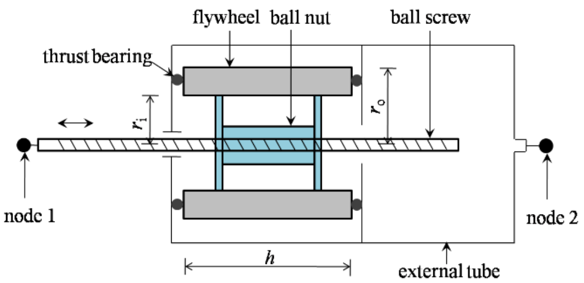

Fig. 1 Schematic of the ball screw inerter

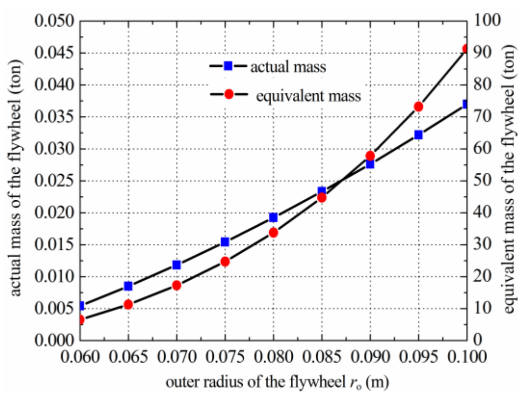

Fig. 2 Variation of the actual mass and apparent mass of a flywheel with its outer radius

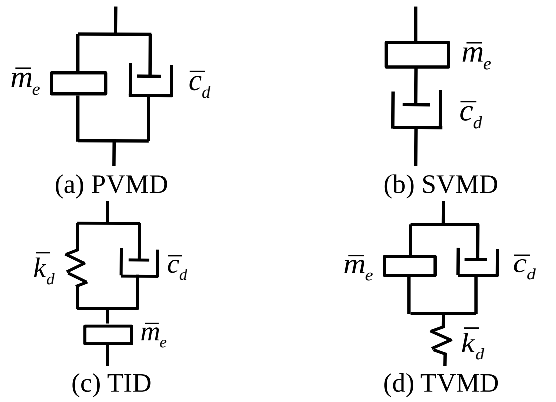

Fig.3 The mechanical model of the employed IBDDs

It can be seen that the apparent mass of this inerter is more than 1000 times of its actual mass. Especially, when r_o is larger than 0.08 m the apparent mass is beyond 30ton, which is about half of the total mass of a 600 m long stay cable (the mass of per unit length of the stay cable is assumed to be 100 kg/m). Since the actual mass of the inerter employed in cable applications is only about tens of kilograms, it will not cause cable sag.

2.2 Inerter-based damping devices (IBDDs)

As the inerter itself does not dissipate any energy of vibration, damping elements are always employed together with the inerter to form a compound passive energy damping device, called the inerter-based damping device. The mechanical models of the four IBDDs employed in this study are shown in Figs. 3(a)-3(d), where $\overline{c}_d$ is the damping coefficient of the linear viscous damper; $\overline{k}_d$ is the stiffness of the supporting spring. Fig. 3(a) is PVMD, which consists of an inerter and a viscous damper in parallel configuration and is also called viscous mass damper (VMD) (Ikago *et al*. 2012) or viscous inertial mass damper (VIMD) (Lu *et al.* 2017). Fig. 3(b) is the SVMD, and it is composed of an inerter and a viscous damper in series configuration. The configurations of TID (Lazar *et al.* 2016) and TVMD (Ikago *et al.* 2012) are shown in Figs. 3(c) and 3(d), respectively.

It is worth to mention that for PVMD the inerter and the viscous damper can be easily integrated in one device, such as the design of VMD and the electromagnetic inertial mass damper (EIMD) (Nakamura *et al*. 2014). Therefore, the configuration of the PVMD may be as simple as that of the traditional viscous damper, and their cost may be comparable. On the other hand, the integration of the TID and SVMD seems more difficult. Both fluid dampers and eddy current dampers can be used to integrate with inerter for engineering applications (Ikago *et al.* 2012, Chen *et al.* 2015).

3. Formulation of Cable - IBDD system

Many advanced models of cable-damper system have been proposed in the past decades, in which the cable is modeled as a tensioned beam with static deformation and the support conditions of damper are also taken into account. However, in this study the cable is still modeled as a taut string due to the feasibility and practical considerations. Moreover, because the relevant excitation mechanisms of the stay cable are complex, free vibration is considered at the first stage and the supplemental modal damping ratio is used as the performance index for the four IBDDs. Forced vibration analysis is also considered in the last section to further examine the effectiveness of PVMD for multi-mode cable vibration control.

The state-space equation of the cable-TID system (Fig. 4) will be derived below as an illustration for the general cable-IBDD system. The natural damping of the cable is neglected. The IBDD location is assumed to be near the cable anchorage in the range of 1%~5% of the cable length. Under these assumptions, the governing dimensionless equation of in-plane vibration of the cable–TID system is given by

$$\begin{cases} \ddot{v}(x,t) - \dfrac{1}{\pi^2} v''(x,t) = F_d \cdot \delta(x - x_d) + f(x,t) \\ F_d = c_d[\dot{y} - \dot{v}(x_d)] + k_d[y - v(x_d)] = -m_e \ddot{y} \end{cases} \tag{7}$$

where v is the transverse deflection of the cable; y is the displacement of the inerter relative to the base; x is the coordinate originating from the left end of the cable; x_d is the damper position; k_d is the stiffness of the supporting spring; c_d is the damping coefficient of the viscous damper; m_e is the apparent mass of the inerter; F_d is the total control force; $f(x,t)$ is the distribution force on the cable; δ is the Dirac delta function; prime and dot are partial derivatives with respect to location x and time t, respectively. The dimensional counterparts of the previous dimensionless quantities are shown with over bars, and their relationships are given below

$$\begin{gathered} t = \omega_1 \bar{t} \quad x = \bar{x}/L \quad y = \bar{y}/L \\ v(x,t) = v(\bar{x}, \bar{t})/L \quad \delta(x - x_d) = L\delta(\bar{x} - \bar{x}_d) \\ f(x,t) = L\bar{f}(\bar{x}, \bar{t})/\pi^2 T \quad F_d = \bar{F}_d(\bar{t})/\pi^2 T \\ m_e = \frac{\bar{m}_e L \omega_1^2}{\pi^2 T} \quad k_d = \frac{\bar{k}_d L \omega_1}{\pi^2 T} \quad c_d = \frac{\bar{c}_d L \omega_1}{\pi^2 T} \quad \omega_1 = \frac{\pi}{L}\sqrt{\frac{T}{\rho}} \end{gathered} \tag{8}$$

where T is the cable tension; L is the cable length; ω_1 is the fundamental natural frequency of the undamped cable; ρ is the cable mass per unit length.

For TID and TVMD, it is more conventional to use the mass ratio $\mu = \bar{m}_e/\rho L$, frequency ratio $\alpha = \omega_d/\omega_1$ and damping ratio $\xi_d = \bar{c}_d/2\bar{m}_e\omega_d$ to describe their dynamic characteristics, where $\omega_d = \sqrt{\bar{k}_d/\bar{m}_e}$ denotes the natural frequency of TID and TVMD. These quantities can also be related to m_e, c_d and k_d by taking some manipulations of Eq. (7)

$$m_e = \mu \quad k_d = \mu\alpha^2 \quad c_d = 2\mu\alpha\xi_d \tag{9}$$

where $m_e = \mu$ is also valid for PVMD and SVMD, so m_e also represents the mass ratio between the IBDDs and the cable.

The transverse deflection may be approximated by a finite series

$$v(x,t) = \sum_{j=1}^{m} q_j(t) \cdot \phi_j(x) \tag{10}$$

where $q_j(t)$ is the jth generalized displacements; $\phi_j(x)$ is the jth shape function given by Johnson *et al.* (2007)

$$\begin{gathered} \phi_1 = \begin{cases} x/x_d & 0 \leqslant x \leqslant x_d \\ (1-x)/(1-x_d) & x_d < x \leqslant 1 \end{cases} \\ \phi_{j+1}(x) = \sin \pi j x \quad j \geqslant 1 \end{gathered} \tag{11}$$

where $\phi_1(x)$ is the shape function considering the cable deflection due to a static force at the damper location. It is introduced here to decrease the number of terms required for comparable accuracy. In this paper m is set to be 21 according to the previous study (Johnson *et al*. 2007).

Following the procedure given by Johnson *et al.* (2007), the equation of motion in a matrix form can be obtained as

$$\begin{bmatrix} \boldsymbol{M} & \mathbf{0}_{1\times 21} \\ \mathbf{0}_{21\times 1} & m_e \end{bmatrix} \begin{Bmatrix} \ddot{\boldsymbol{q}}(t) \\ \ddot{y} \end{Bmatrix} + \begin{bmatrix} \boldsymbol{C}_d & -\boldsymbol{c}_1 \\ -\boldsymbol{c}_1^T & c_d \end{bmatrix} \begin{Bmatrix} \dot{\boldsymbol{q}}(t) \\ \dot{y} \end{Bmatrix} + \begin{bmatrix} \boldsymbol{K} + \boldsymbol{K}_d & -\boldsymbol{k}_1 \\ -\boldsymbol{k}_1^T & k_d \end{bmatrix} \begin{Bmatrix} \boldsymbol{q}(t) \\ y \end{Bmatrix} = \begin{Bmatrix} \boldsymbol{f} \\ 0 \end{Bmatrix} \tag{12}$$

where the mass matrix $\boldsymbol{M}=[m_{ij}]$, the stiffness matrix $\boldsymbol{K}=[k_{ij}]$, the damping vector related to the damper $\boldsymbol{c}_1=c_d\boldsymbol{\phi}(x_d)= c_d\boldsymbol{\varphi}$ the damping matrix related to the damper $\boldsymbol{C}_d=\boldsymbol{\varphi}^T c_d \boldsymbol{\varphi}$, the stiffness vector related to the damper $\boldsymbol{k}_1=k_d\boldsymbol{\varphi}$, the stiffness matrix related to the damper $\boldsymbol{K}_d=\boldsymbol{\varphi}^T k_d \boldsymbol{\varphi}$; $\boldsymbol{f}$ is the external load vector. Each element of these matrices and vectors can be determined as

$$\begin{gathered} m_{ij} = \int_0^1 \phi_i(x)\phi_j(x)dx \quad k_{ij} = -\frac{1}{\pi^2}\int_0^1 \phi_i(x)\phi_j''(x)dx \\ f_i = \int_0^1 f(x,t)\phi_i(x)dx \quad \boldsymbol{\varphi} = [\phi_1(x_d), \phi_2(x_d), ..., \phi_m(x_d)]^T \end{gathered} \tag{13}$$

Equivalently, the state-space representation of Eq. (12) can be formulated as

$$\begin{bmatrix} \dot{\boldsymbol{q}}_1 \\ \ddot{\boldsymbol{q}}_1 \end{bmatrix} = \begin{bmatrix} \mathbf{0}_{22\times 22} & \boldsymbol{I}_{22\times 22} \\ -\boldsymbol{M}_s^{-1}\boldsymbol{K}_s & -\boldsymbol{M}_s^{-1}\boldsymbol{C}_s \end{bmatrix} \begin{bmatrix} \boldsymbol{q}_1 \\ \dot{\boldsymbol{q}}_1 \end{bmatrix} + \begin{bmatrix} \mathbf{0}_{22\times 22} \\ \boldsymbol{M}_s^{-1} \end{bmatrix} \boldsymbol{g} \tag{14}$$

where

$$\begin{gathered} \begin{Bmatrix} \boldsymbol{q}(t) \\ y \end{Bmatrix} = \boldsymbol{q}_1(t) \quad \begin{Bmatrix} \boldsymbol{f} \\ 0 \end{Bmatrix} = \boldsymbol{g} \quad \boldsymbol{M}_s = \begin{bmatrix} \boldsymbol{M} & \mathbf{0}_{1\times 21} \\ 0_{21\times 1} & m_e \end{bmatrix} \\ \boldsymbol{C}_s = \begin{bmatrix} \boldsymbol{C}_d & -\boldsymbol{c}_1 \\ -\boldsymbol{c}_1^T & c_d \end{bmatrix} \quad \boldsymbol{K}_s = \begin{bmatrix} \boldsymbol{K} + \boldsymbol{K}_d & -\boldsymbol{k}_1 \\ -\boldsymbol{k}_1^T & k_d \end{bmatrix} \end{gathered} \tag{15}$$

For free vibration $\boldsymbol{f}$=0, thus complex modal analysis can be conducted for Eq. (13), and the modal shape and modal damping ratio for the first several modes of the cable-TID system can be derived from the corresponding eigenvectors and eigenvalues, respectively. The eigenvalues are complex in general and have the form below

$$\lambda_j = \frac{\omega_j}{\omega_1}\left(1 \pm i\sqrt{1-\xi_j^2}\right) \tag{16}$$

where ω_j denotes the jth modal frequency of the dimensional cable-TID system; ξ_j denotes the jth modal damping ratio. As pointed out by Lu *et al.* (2017), the installation of PVMD will introduce a frequency-shifting mode, which is not critical in the cable vibration problem since it always has higher damping ratio compared with the other modes. This conclusion also holds for SVMD, TID and TVMD. Thus the shifting mode will not be discussed below for all the IBDDs in this paper.

For forced vibration, the cable displacement response and the control force are usually used as the performance indices. Based on the state-space method they can be formulated in frequency domain as

$$\boldsymbol{Y}(j\omega) = [\boldsymbol{C}(j\omega\boldsymbol{I}-\boldsymbol{A})^{-1}\boldsymbol{B}+\boldsymbol{D}]\boldsymbol{G}(j\omega) \tag{17}$$

where $\boldsymbol{Y}$(jω) is the Fourier transform of the output vector $\boldsymbol{y}=\{v(x_i,t),\ F_d\}^T$; $\boldsymbol{G}$ is the Fourier transform of the external load vector $\boldsymbol{g}$; $\boldsymbol{A}$, $\boldsymbol{B}$, $\boldsymbol{C}$ and $\boldsymbol{D}$ are given by

$$\boldsymbol{A} = \begin{bmatrix} \boldsymbol{0}_{22\times22} & \boldsymbol{I}_{22\times22} \\ -\boldsymbol{M}_s^{-1}\boldsymbol{K}_s & -\boldsymbol{M}_s^{-1}\boldsymbol{C}_s \end{bmatrix} \quad \boldsymbol{B} = \begin{bmatrix} \boldsymbol{0}_{22\times22} \\ \boldsymbol{M}_s^{-1} \end{bmatrix}$$
$$\boldsymbol{C} = \begin{bmatrix} [\boldsymbol{\phi}^T(x_i)\ \ 0] & \boldsymbol{0}_{1\times22}^T \\ [-k_d\boldsymbol{\varphi}^T\ \ k_d] & [-c_d\boldsymbol{\varphi}^T\ \ c_d] \end{bmatrix} \quad \boldsymbol{D}_s = \begin{bmatrix} \boldsymbol{0}_{1\times22}^T \\ \boldsymbol{0}_{1\times22}^T \end{bmatrix} \tag{18}$$

where x_i denotes the location where the cable displacement response is calculated. It is worth to mention that the state-space equations for cable-PVMD system, cable-SVMD system and cable-TVMD can be derived in the same way, but they are different with each other.

4. Single-mode vibration control of cable based on IBDDs

For single-mode vibration control the optimization objective is to obtain the maximum damping ratio of the first four modes of the cable/IBBDs system. In this study the Matlab fminsearch function is used to search for the optimum parameters. Fminsearch function utilizes the Nelder-Mead simplex algorithm to solve the unconstrained optimization problem by a direct search method (Lagarias *et al.* 1998). During the optimization procedure fminsearch function keeps calling the objective function, which calculates the damping ratio for a certain mode, until the tolerance on the optimal parameters reaches 1.0e-8.

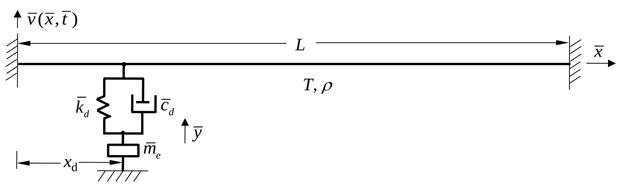

Fig. 4 Taut cable with the TID

4.1 Parametric optimization for PVMD and SVMD

The maximum attainable damping ratios of the cable/PVMD system and cable-SVMD system are presented in Table 1 for the first four modes and the dimensionless damper location, x_d, in the range of 0.01~0.05. It can be seen that for both PVMD and SVMD, the maximum attainable damping ratio increases as the dimensionless damper location increases, and decreases as the mode number increases. For the same damper location and mode number, the maximum attainable damping ratio of the cable-SVMD system is always slightly larger than that of the cable-PVMD system. The maximum attainable damping ratios for cable-viscous damper (VD) system estimated from Krenk (2000) are given in Table 4 for comparison. It can be seen that PVMD and SVMD performs much better than VD. For x_d=0.01, which may happen in the case of super-long cable vibration control, the maximum attainable damping ratios of the cable-PVMD system and the cable-SVMD system are up to ten times of those of the cable-VD system.

The optimal values of the dimensionless apparent masses of PVMD and SVMD are shown in Table 2. For both PVMD and SVMD, the optimal dimensionless apparent mass is approximately proportional to the dimensionless damper location and inversely proportional to the square of the mode number. For the same damper location and mode number, the optimal dimensionless apparent mass of PVMD is always smaller than that of SVMD, and this difference increases with the increasing damper location and mode number. It can be observed that when x_d=0.05 the optimal dimensionless apparent mass of PVMD is only a half of that of the SVMD for the fourth mode.

The optimal dimensionless damping coefficients of PVMD and SVMD are compared in Table 3. For both PVMD and SVMD, the optimal dimensionless damping coefficient decreases as the damper location and mode number increase alone or in combination. For the same damper location and mode number, the optimal dimensionless damping coefficient of PVMD is always much smaller than that of SVMD, and this difference increases with the decreasing damper location and mode number. In the case of x_d=0.01, the optimal dimensionless damping coefficients of PVMD are just 10% of those of SVMD for all the first four modes. The optimal dimensionless damping coefficient of VD is also given in Table 4 for comparison. It can be seen that the optimal dimensionless damping coefficient of PVMD for each mode and damper location is always smaller than that of VD, whereas the reverse is valid for SVMD. Therefore, the size of PVMD can be smaller than that of VD if only the damping element is considered.

In order to validate the results of numerical optimization, the damping ratio distribution contours of the first mode of the cable-PVMD system and the cable-SVMD system are given in Figs. 5 and 6, respectively. It can be seen that for both PVMD and SVMD the optimal dimensionless apparent masses and damping coefficients agree well with those shown in Tables 2 and 3. Moreover, it can be concluded that the parametric optimizations of PVMD and SVMD are convex problems, thus

Table 1 Maximum attainable damping ratio of cable-PVMD system and cable-SVMD system

x_d	Cable-PVMD system				Cable-SVMD system			
	Mode 1	Mode 2	Mode 3	Mode 4	Mode 1	Mode 2	Mode 3	Mode 4
0.01	0.0704	0.0681	0.0662	0.0633	0.0706	0.0692	0.0670	0.0644
0.02	0.0994	0.0952	0.0897	0.0839	0.1000	0.0965	0.0915	0.0865
0.03	0.1219	0.1146	0.1046	0.0976	0.1229	0.1173	0.1100	0.1025
0.04	0.1405	0.1297	0.1178	0.1076	0.1426	0.1348	0.1256	0.1164
0.05	0.1570	0.1407	0.1284	0.1154	0.1604	0.1511	0.1394	0.1291

Table 2 Optimal dimensionless apparent mass of PVMD and SVMD

x_d	Cable-PVMD system				Cable-SVMD system			
	Mode 1	Mode 2	Mode 3	Mode 4	Mode 1	Mode 2	Mode 3	Mode 4
0.01	9.8777	2.4674	1.0951	0.6148	10.2974	2.5823	1.1534	0.653
0.02	4.8104	1.1986	0.5295	0.2952	5.2449	1.3271	0.6009	0.3465
0.03	3.1206	0.774	0.339	0.1866	3.5702	0.9165	0.4245	0.2521
0.04	2.275	0.5603	0.2422	0.1306	2.7402	0.7175	0.3431	0.2127
0.05	1.7672	0.4312	0.1829	0.0956	2.2485	0.6043	0.3003	0.1971

Table 3 Optimal dimensionless damping coefficient of PVMD and SVMD

x_d	Cable-PVMD system				Cable-SVMD system			
	Mode 1	Mode 2	Mode 3	Mode 4	Mode 1	Mode 2	Mode 3	Mode 4
0.01	2.860	1.450	1.010	0.790	35.820	17.550	11.330	8.180
0.02	2.025	1.060	0.755	0.610	12.695	6.130	3.890	2.750
0.03	1.659	0.887	0.640	0.537	6.933	3.323	2.087	1.470
0.04	1.440	0.783	0.583	0.493	4.530	2.168	1.358	0.960
0.05	1.288	0.708	0.542	0.464	3.266	1.562	0.990	0.710

Table 4 Optimal parameters of cable-VD system

x_d	Optimum damping coefficient				Maximum attainable damping ratio			
	Mode 1	Mode 2	Mode 3	Mode 4	Mode 1	Mode 2	Mode 3	Mode 4
0.01	10.142	5.071	3.381	2.535	0.005	0.005	0.005	0.005
0.02	5.071	2.535	1.690	1.268	0.01	0.01	0.01	0.01
0.03	3.38	1.690	1.127	0.845	0.015	0.015	0.015	0.015
0.04	2.535	1.268	0.845	0.634	0.02	0.02	0.02	0.02
0.05	2.028	1.014	0.676	0.507	0.025	0.025	0.025	0.025

the Nelder-Mead simplex algorithm used in this study is stable and can converge to the optimal solutions very fast. Additionally, It is worth to mention that for x_d=0.02, the optimal parameters of PVMD and the corresponding maximum attainable damping ratios agree very well with those obtained by Lu *et al.* (2017) using the direct ergodic search method.

Based on the previous comparisons between PVMD and SVMD, one can conclude that PVMD is more effective than SVMD for cable vibration control. However, it is worth noting that even a PVMD is installed at 5% of the cable length, its optimal dimensionless apparent mass for the first mode is still too large to be realized by an inerter with a practically reasonable size if the super-long cable vibration control is considered. Therefore, a non-optimal apparent mass, which is small enough to keep the inerter in suitable size without conflicting with the aesthetics of the bridge, has to be used in practical design. On the other hand, the optimal parameters are not necessary if the required modal damping ratio can be obtained by a non-optimal apparent mass.

Table 5 Maximum attainable damping ratio of cable-TID system and cable-TVMD system

$\mu(m_e)$	x_d=0.01		x_d =0.02		x_d =0.03		x_d =0.04		x_d =0.05	
	TID	TVMD	TID	TVMD	TID	TVMD	TID	TVMD	TID	TVMD
0.1	0.0069	0.0070	0.0138	0.0140	0.0210	0.0209	0.0280	0.0278	0.0348	0.0348
0.2	0.0097	0.0096	0.0195	0.0196	0.0295	0.0295	0.0395	0.0395	0.0492	0.0496
0.3	0.0119	0.0114	0.0240	0.0240	0.0360	0.0365	0.0484	0.0487	0.0604	0.0610
0.4	0.0139	0.0137	0.0279	0.0279	0.0417	0.0420	0.0559	0.0562	0.0700	0.0708
0.5	0.0154	0.0155	0.0313	0.0314	0.0468	0.0470	0.0625	0.0631	0.0787	0.0793

Table 6 Optimal frequency ratio of TID and TVMD

$\mu(m_e)$	x_d=0.01		x_d =0.02		x_d =0.03		x_d =0.04		x_d =0.05	
	TID	TVMD	TID	TVMD	TID	TVMD	TID	TVMD	TID	TVMD
0.1	1.0047	1.0051	1.0088	1.0105	1.0124	1.0162	1.0153	1.0222	1.0175	1.0286
0.2	1.0094	1.0102	1.0179	1.0213	1.0250	1.0333	1.0307	1.0461	1.0347	1.0598
0.3	1.0142	1.0155	1.027	1.0325	1.0379	1.0512	1.0461	1.0717	1.0513	1.0942
0.4	1.0191	1.0209	1.0364	1.0441	1.0508	1.0701	1.0614	1.0993	1.0669	1.1323
0.5	1.024	1.0263	1.0459	1.0561	1.0640	1.0901	1.0764	1.1293	1.0810	1.1748

Table 7 Optimal damping ratio of TID and TVMD

$\mu(m_e)$	x_d=0.01		x_d =0.02		x_d =0.03		x_d =0.04		x_d =0.05	
	TID	TVMD	TID	TVMD	TID	TVMD	TID	TVMD	TID	TVMD
0.1	0.0014	0.0014	0.0058	0.0056	0.0089	0.0084	0.0120	0.0112	0.0152	0.0141
0.2	0.0039	0.0039	0.0171	0.0159	0.0265	0.0239	0.0365	0.0320	0.0468	0.0403
0.3	0.0072	0.0069	0.0326	0.0292	0.0514	0.0442	0.0722	0.0592	0.0937	0.0741
0.4	0.0114	0.0112	0.0523	0.0451	0.0842	0.0682	0.1193	0.0917	0.1574	0.1163
0.5	0.0158	0.0159	0.0761	0.0633	0.1245	0.0955	0.1793	0.1291	0.2399	0.1641

4.2 Parametric optimization for TID and TVMD

Because both TID and TVMD have the narrow band control characteristics, only the vibration control of the fundamental mode is considered in this paper. For TID and TVMD, there are three parameters, namely mass ratio, frequency ratio and damping ratio. It is known that the protection efficiency of TID and TVMD against vibration grows monotonically with the mass ratio, so only the frequency ratio and damping ratio are considered here as design variables, while the mass ratio is assumed to be a constant design parameter. The mass ratio m_e is assumed to be in the range of 0.1~0.5. Matlab-based Nelder-Mead simplex algorithm is conducted to find the optimum solutions for TID and TVMD.

The comparison of the maximum attainable damping ratios for cable-TID system and cable-TVMD system are provided in Table 5. It is found that for the same mass ratio and damper location, the maximum attainable damping ratios of the cable-TID system are almost the same as those of the cable-TVMD system. For both TID and TVMD, the maximum attainable damping ratio increases as the dimensionless damper location and the mass ratio increase. It is noted that the increasing ratio of the maximum attainable damping ratio decreases with the increasing mass ratio, so it is not efficient to use a mass ratio larger than 0.5.

Based on Table 1, Tables 4 and 5, performance comparison can be carried out for TID, TVMD, PVMD, SVMD and VD for the first-mode vibration control. It can be seen that both TID and TVMD can providing more damping to the cable than the viscous damper does if their mass ratios are larger than 0.1. On the other hand, the maximum attainable damping ratios of the cable-PVMD system and cable-SVMD system are much larger than those of the cable-TID system and cable-TVMD system.

The optimal frequency ratios of TID and TVMD are shown in Table 6. It can be observed that the optimal frequency ratio of TVMD is always slightly larger than that of TID. In addition, for both TID and TVMD, the optimal frequency ratio increases as the dimensionless mass ratio increases. The optimal damping ratios of TID and TVMD are shown in Table 7, while the corresponding optimal damping coefficient can be obtained using Eq. (9). The results show that the optimal damping coefficients of TID and TVMD are much smaller than those of PVMD, so the size of the viscous damper used in TVMD and TID can be significantly reduced.

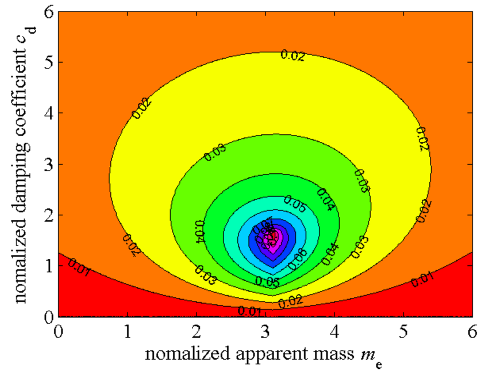

Fig. 5 Damping ratio distribution contour for PVMD (mode 1, x_d=0.03)

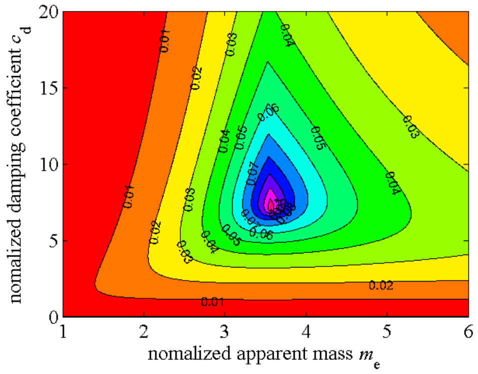

Fig. 6 Damping ratio distribution contour for SVMD (mode 1, x_d=0.03)

5. Multi-mode vibration control of cable based on PVMD

Due to the uncertainty of the predominant mode of the rain-wind induced stay cable vibrations, all the damping ratios of the first several modes have to fulfill Irwin's criterion for minimum Scruton number. However, TID and TVMD are not suitable for multi-mode vibration control due to their frequency tuning requirements. The preceding analysis has shown that PVMD performs much better than SVMD for single-mode vibration control, and it can be integrated in one device much more easily. These factors significantly enhance the feasibility of PVMD in practical application, so in this section only PVMD will be studied for the multi-mode vibration of cable.

5.1 Parametric analysis of PVMD

For super-long stay cable the dimensionless damper location x_d can be assumed to be 0.02, thus as shown in Table 2 the optimal dimensionless apparent masses of PVMD are 4.8104, 1.1986, 0.5295 and 0.2952 for the first four modes, respectively. If we assume that the stay cable is 600 m long and 100 kg per unit length, the corresponding optimal apparent masses of PVMD are 288.624ton, 71.9ton, 31.77ton and 17.7ton, respectively, for the first four modes. Obviously, the first case is not feasible in practice , since the outer radius of the flywheel will be too large as shown in Fig. 2. Therefore, for super-long cable vibration control it is reasonable to assume that the dimensionless apparent mass of PVMD is in the range of 0~0.5. In this case the size of the PVMD can be comparable with the traditional viscous damper.

The variations of the modal damping ratios with the dimensionless damping coefficients of PVMD for m_e=0.1 and m_e=0.5 are shown in Figs. 7(a) and 7(b), respectively. It can be observed that for a given apparent mass there is an optimal damping coefficient for each of the first four modes to obtain a maximum modal damping ratio. Since the optimum damping coefficients and the maximum modal damping ratios shown in Fig. 7 are corresponding to a non-optimal apparent mass, they are referred to as suboptimum damping coefficient and suboptimal modal damping ratio, respectively. Obviously, the suboptimal damping coefficient and the suboptimal modal damping ratio depend on the apparent mass.

In order to achieve a better understanding of the influence of the apparent mass on the performance of PVMD, the variations of the suboptimal maximum damping ratio and suboptimal damping coefficient with the dimensionless apparent mass is shown in Figs. 8(a) and 8(b), respectively.

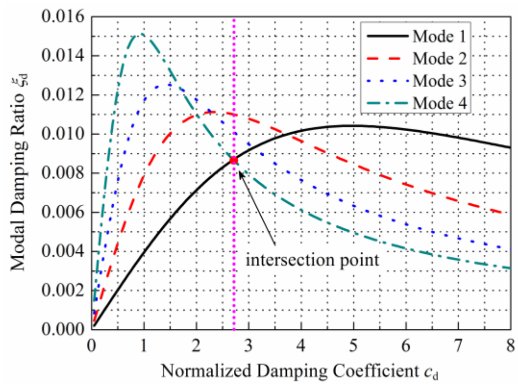

(a) m_e=0.1

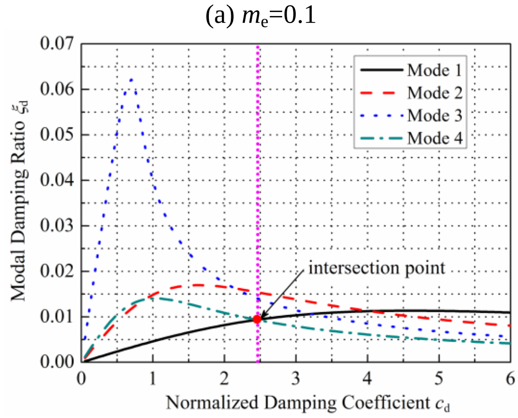

(b) m_e=0.5

Fig. 7 Modal damping ratio curves of the cable-PVMD system with nonoptimal apparent mass, x_d=0.02

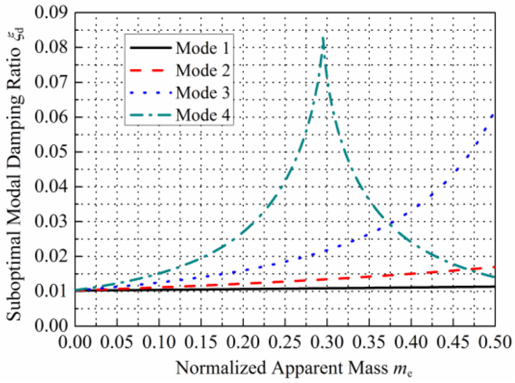

(a) variation of the suboptimal modal damping ratio with dimensionless apparent mass

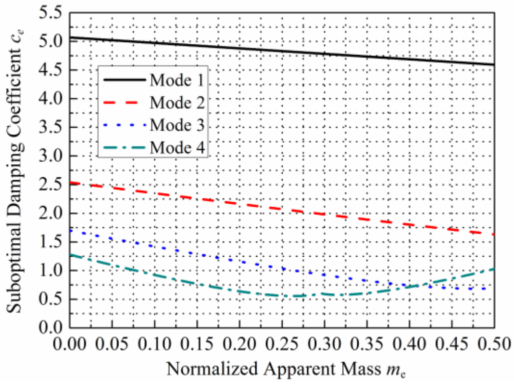

(b) variation of the suboptimal damping coefficient with dimensionless apparent mass

Fig. 8 Influence of the apparent mass on PVMD performance

It can be seen from Fig. 8(a) that with help of inerter PVMD can always improve the maximum attainable damping ratio of the first four modes compared with the traditional VD. For the fourth mode, the suboptimal maximum damping ratio firstly increases with the apparent mass and reaches its maximum at the optimal apparent mass, and then it decreases as the apparent mass continuously increases. It is worth to point out that the optimal dimensionless apparent masses of the first two modes are much larger than 0.5, so the improvements of the damping ratios of mode 1 and mode 2 are very small as shown in Fig. 8(a). For example, when m_e=0.5 the suboptimal modal damping ratios of mode 1 and mode 2 increase by 11.3% and 66.4%, respectively, compared with the maximum attainable damping ratio of VD. In addition, it is found that in case of x_d=0.02 TID and TVMD can provide significantly larger damping ratio than PVMD does if the upper limit of mass ratio is assumed to be 0.5.

It can be observed from Fig. 8(b) that the suboptimum damping coefficients of the first four modes are always smaller than that of VD. For the first three modes, the suboptimal damping coefficient decreases almost linearly with the increasing apparent mass. For the fourth mode, the suboptimal damping coefficient reaches its minimum near the optimum apparent mass.

5.2 Parametric optimization of PVMD

Fig. 7 has shown that for a given apparent mass the suboptimal damping coefficients of the first four modes are different from each other, so it is favorable to select a dimensionless damping coefficient that can maximizes the minimal modal damping ratio of the first four modes. As a result, almost minimum variance of the damping ratios of the first four modes can be obtained. This favorable design principle can be defined as a constrained minimax problem, and the intersection point shown in Figs. 7(a) and 7(b) just represents the solution of this problem for m_e=0.1 and m_e=0.5, respectively. It is worth to mention that similar design methods have been proposed by Xu and Zhou (2007) and Weber *et al*. (2009) to design other dampers for multi-mode cable vibration control.

The Matlab function fminimax is employed to solve the constrained minimax problem. The favorable dimensionless damping coefficients and the corresponding modal damping ratios of the first four modes are displayed in Figs. 9(a) and 9(b), respectively. It can be seen that the favorable dimensionless damping coefficient is between 2.4 and 2.8 when the apparent mass falls in the range of 0~0.5. Particularly, when the apparent mass is less than 0.4 the favorable damping coefficient of PVMD is slightly larger than that of VD. Fig. 9(b) indicates that all the modal damping ratios of the first four modes increase gradually with the increasing apparent mass, but the increasing rates of the second mode and the third mode are more significant than those of the mode 1 and the mode 4.

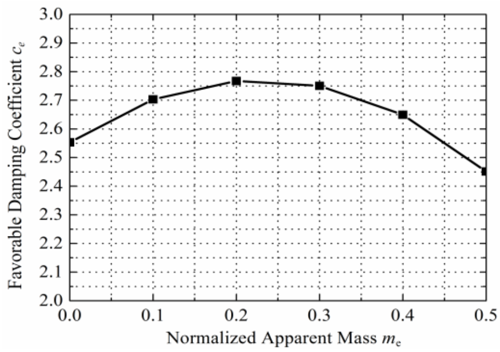

(a) Favorable damping coefficient vs dimensionless apparent mass

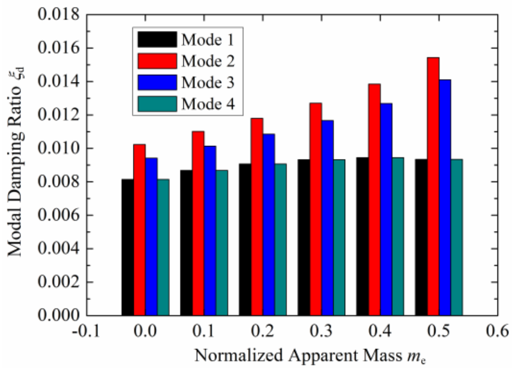

(b) Modal damping ratios of the first four modes vs dimensionless apparent mass

Fig. 9 Optimum parameters of PVMD for multi-mode vibration control

For example, in the case of VD the damping ratios of the first four modes are 0.814%, 1.002%, 0.942% and 0.814%, respectively, while in the case of PVMD with me=0.5, they are 0.934%,1.543%,1.414% and 0.934%, respectively. Thus the improvements of the damping ratio are approximate 15% for mode 1 and mode 4 and 50% for mode 2 and mode 3.

5.3 control of cable vibration under sinusoidal excitation

The performance of PVMD can be further examined by forced vibration analysis, in which the steady-state displacement response of the cable at midspan and the control force are used as the performance indices. The N313 cable on Stonecutters Bridge is chosen for simulation (Lu *et al.* 2017). The length and the mass of per unit length of N313 cable are 306.69 m and 98.6 Kg/m^3, respectively. The tension force is 5529.6 KN, resulting in a fundamental frequency f_1=0.386 Hz. To avoid infinite resonance peaks of the cable in the case without PVMD, a small internal damping coefficient c=2 N•s/m^2 is introduced in the calculations to the forced vibrations of the cable with and without PVMD. The dimensionless damper location is assumed to be x_d=0.02. Uniformly distributed harmonic loads are assumed, the amplitude of the load is f=2 N/m, acting in the cable plane. The dimensionless apparent mass of PVMD is assumed to be m_e=0.5, corresponding to a dimension mass of 15.120 ton. The damping coefficient of PVMD is calculated from the parametric optimization of multi-mode vibration control, that is $\bar{c}_d$=179.833 KN•s/m^2. For comparison, the optimal PVMD (m_e=4.8104, c_d=2.025) for single-mode vibration control, the optimal VD (c_d=2.55) for multi-mode vibration control and the optimal VD (c_d=5.071) for single mode control are also considered in the forced vibration analysis.

The displacement frequency response of the cable at midspan and the control force frequency response are calculated from Eq. (16), and the results are shown in Figs. 10 and 11, respectively. It can be seen from both figures that within the displayed excitation frequency range, only the first two natural frequencies corresponding to the first two symmetric modes are excited out, because symmetric harmonic loads are considered. It can be observed from Fig. 10 that the PVMD designed for multi-mode vibration control (PVMD-M) can significantly suppress the resonance peaks of both mode 1 and mode 3, while the PVMD designed for the first mode vibration control (PVMD-S) is not able to generate enough suppression on the resonance peak of mode 3. Moreover, if the same design strategy is employed, PVMD always performs better than VD. These are consistent with the results from the modal damping ratio analysis.

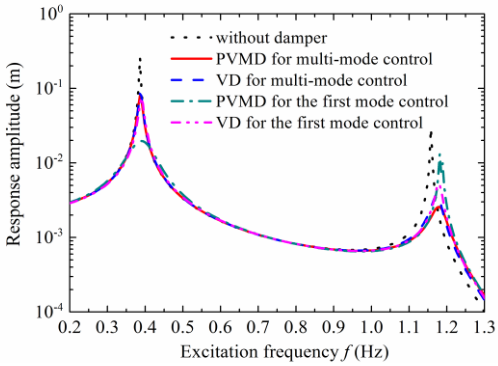

Fig. 10 Displacement frequency response of the cable at the middle span, x_d=0.02

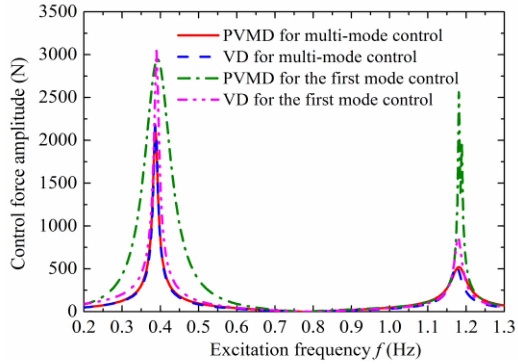

Fig. 11 Control force frequency response, x_d=0.02

As for the control force, it can be seen from Fig. 11 that PVMD-M produces much less control force compared with PVMD-S. Especially at the resonant frequency of mode 3, the peak control force produced by PVMD-S is nearly five times of that produced by PVMD-M. This is because that the apparent mass of PVMD-S is so large that the inertial force produced by the inerter under higher frequency excitation is significantly amplified. That is to say PVMD can benefit from the multi-mode vibration control strategy, in which excessive control force can be avoided under high frequency vibration. Moreover, the peak control forces of PVMD and VD are almost the same under multi-mode control strategy, this means that a parallel connected inerter can improve the performance of a traditional VD without increasing the total control force.

6. Conclusions

In this paper, the performances of four different kinds of IBDDs, including PVMD, SVMD, TID and TVMD, are studied for suppression of cable vibration. For single-mode vibration control, all of the four IBDDs are proved to be more effective than the traditional viscous damper. PVMD performs better than SVMD, because it is able to provide nearly the same maximum attainable damping ratio for the cable-damper system as SVMD does, but its optimal apparent mass and optimal damping coefficient are significantly smaller. The maximum attainable damping ratios of the first mode for both cable-PVMD system and cable-SVMD system are much larger than those of the cable-TID system and cable-TVMD system. However, if the dimensionless apparent masses of all the four IBBDs are limited in the range of 0~0.5, both TID and TVMD outperform PVMD and SVMD. For multi-mode vibration control based on PVMD, the modal damping ratios of all the first four modes can be increased compared with VD and the increment increases with the increasing apparent mass. The results of damping ratio analysis are also examined through a forced vibration analysis by numerical simulation, and the results show that PVMD can benefit from the multi-mode vibration control strategy, in which excessive control force can be avoided under high frequency vibration. The results of this study clearly demonstrate the effectiveness and advantages of IBBDs, especially PVMD, in cable vibration control.

It is noted that the IBBDs considered in this paper can only be used for passive vibration control. However, if the apparent mass of the inerter can be adaptively adjusted by changing the moment of inertia of the flywheel, then semi active or active control can be implemented by IBDDs and much better control performance can be expected for multi-mode vibration control.

Acknowledgments

The authors would like to acknowledge support from the National Science Foundation of China (No. 51808210) and from the State's Key Project of Research and Development Plan (No. 2016YFE0127900).

References

Chen, L., Sun, L.M. and Nagarajaiah, S. (2015), "Cable with discrete negative stiffness device and viscous damper: Passive realization and general characteristics", *Smart. Struct. Syst.*, **15**(3), 627-643. http://dx.doi.org/10.12989/sss.2015.15.3.627.

Chen, M.Z.Q., Hu, Y.L., Li, C.Y. and Chen, G.R. (2015), "Performance benefits of using inerter in semiactive suspensions", *IEEE T. Contr. Syst. T*, **23**(4), 1571-1577. doi: 10.1109/TCST.2014.2364954

Chen, M.Z., Papageorgiou, C., Scheibe, F., Wang, F.C. and Smith, M.C. (2009), "The missing mechanical circuit element", *IEEE Circuits Syst. Magazine*, **9**(1), 10-26. doi: 10.1109/MCAS.2008.931738

Chen, Z.Q., Wang, X.Y., Ko, J.M., Ni, Y.Q., Spencer B.F., Jr., Yang, G. and Hu, J.H. (2004), "Mr damping system for mitigating wind-rain induced vibration on dongting lake cable-stayed bridge", *Wind Struct.*, **7**(5), 293-304.

Chen, Z.Q., Huang, Z.W. and Hua X.G. (2015), "Inerter-damper-spring passive vibraiton control: its system reliazation with eddy-current mass dampers", *Proceedings of the 14th World Conference on Seismic Isolation, Energy dissipation and active control of Structures*, 9-11 September 2015, San Diego, USA.

Duan, Y.F., Ni, Y.Q., Zhang, H.M., Spencer B.F. and Ko, J.M., (2019b) "Design formulas for vibration control of sagged cables using passive MR dampers", *Smart Struct. Syst.*, Accepted.

Duan, Y.F., Ni, Y.Q., Zhang, H.M., Spencer B.F., Jr. and Ko, J.M., (2019a) "Design formulas for vibration control of taut cables using passive MR dampers", *Smart Struct. Syst.*, Accepted.

Duan Y.F., Tao J.J., Zhang H.M., Wang S.M. and Yun C.B., (2018), "Real-time hybrid simulation based on vector form intrinsic finite element and field programmable gate array", *Struct. Control Health Monit.*, e2277; https://doi.org/10.1002/stc.2277.

Duan, Y.F., Ni, Y.Q. and Ko, J.M. (2005), "State-derivative feedback control of cable vibration using semiactive magnetorheological dampers", *Comput.-Aided Civil Infrastruct. Eng.*, **20**(6), 431-449. https://doi.org/10.1111/j.1467-8667.2005.00396.x.

Duan, Y.F., Ni, Y.Q. and Ko, J.M. (2006), "Cable vibration control using magnetorheological dampers", *J. Intel. Mat. Syst. Str.*, **17**(4), 321-325.

Fournier, J.A. and Cheng, S.H. (2014), "Impact of damper stiffness and damper support stiffness on the efficiency of a linear viscous damper in controlling stay cable vibrations", *J. Bridge Eng.*, **19**(4), 12. https://doi.org/10.1061/(ASCE)BE.1943-5592.0000562.

Fujino, Y. and Hoang, N. (2008), "Design formulas for damping of a stay cable with a damper", *J. Struct. Eng.-ASCE*, **134**(2), 269-278.

Hwang, J.S., Kim, J. and Kim, Y.M. (2007), "Rotational inertia dampers with toggle bracing for vibration control of a building structure", *Eng. Struct.*, **29**(6), 1201-1208. https://doi.org/10.1016/j.engstruct.2006.08.005.

Ikago, K., Saito, K. and Inoue, N. (2012), "Seismic control of single-degree-of-freedom structure using tuned viscous mass damper", *Earthq. Eng. Struct. D.*, **41**(3), 453-474. https://doi.org/10.1002/eqe.1138.

Johnson, E.A., Baker, G.A., Spencer, B.F. Jr. and Fujino, Y. (2007), "Semiactive damping of stay cables", *J. Eng. Mech.-ASCE*, **133**(1), 1-11. https://doi.org/10.1061/(ASCE)0733-9399(2007)133:1(1).

Krenk, S. (2000), "Vibrations of a taut cable with an external damper", *J. Appl. Mech.*, **67**(4), 772.

Krenk, S. and Hogsberg, J.R. (2005), "Damping of cables by a transverse force", *J. Eng. Mech.-ASCE*, **131**(4), 340-348. https://doi.org/10.1061/(ASCE)0733-9399(2005)131:4(340).

Lagarias, J.C., Reeds, J.A., Wright, M.H. and Wright, P.E. (1998), "Convergence properties of the nelder--mead simplex method in low dimensions", *SIAM J. Optim.*, **9**(1), 112-147. https://doi.org/10.1137/S1052623496303470.

Lazar, I.F., Neild, S.A. and Wagg, D.J. (2014), "Using an inerter-based device for structural vibration suppression", *Earthq. Eng. Struct. D.*, **43**(8), 1129-1147. https://doi.org/10.1002/eqe.2390.

Lazar, I.F., Neild, S.A. and Wagg, D.J. (2016), "Vibration suppression of cables using tuned inerter dampers", *Eng. Struct.*, **122**, 62-71. https://doi.org/10.1016/j.engstruct.2016.04.017.

Li, H., Liu, M. and Ou, J.P. (2008), "Negative stiffness characteristics of active and semi-active control systems for stay cables", *Struct. Control. Health Monit.*, **15**(2), 120-142. https://doi.org/10.1002/stc.200.

Li, H., Liu, M., Li, J.H., Guan, X.C. and Ou, J.P. (2007), "Vibration control of stay cables of the shandong binzhou yellow river highway bridge using magnetorheological fluid dampers", *J. Bridge Eng.*, **12**(4), 401-409. https://doi.org/10.1061/(ASCE)1084-0702(2007)12:4(401).

Liu, M., Song, G.B. and Li, H. (2007), "Non-model-based semi-active vibration suppression of stay cables using magneto-rheological fluid dampers", *Smart Mater. Struct.*, **16**(4), 1447-1452.

Lu, L., Duan, Y.F., Spencer, B.F. Jr., Lu, X. and Zhou, Y. (2017), "Inertial mass damper for mitigating cable vibration", *Struct. Control. Health Monit.*, **24**(10), https://doi.org/10.1002/stc.1986.

Luo, J., Jiang, J.Z. and Macdonald, J.H.G. (2016), "Damping performance of taut cables with passive absorbers incorporating inerters", *J. Physics: Conference Series*, **744**(1).

Main, J.A. and Jones, N.P. (2002), "Free vibrations of taut cable with attached damper.I: Linear viscous damper", *J. Eng. Mech.*, **128**(10), 1062-1071. https://doi.org/10.1061/(ASCE)0733-9399(2002)128:10(1062).

Matsumoto, M., Shiraishi, N. and Shirato, H. (1992), “Rain-wind induced vibration of cables of cable-stayed bridges”, *J. Wind Eng. Ind. Aerodyn.*, **43**(1), 2011-2022.

Nakamura, Y., Fukukita, A., Tamura, K., Yamazaki, I., Matsuoka, T., Hiramoto, K. and Sunakoda, K. (2014), “Seismic response control using electromagnetic inertial mass dampers”, *Earthq. Eng. Struct. D.*, **43**(4), 507-527. https://doi.org/10.1002/eqe.2355.

Ni, Y.Q., Chen, Y., Ko, J.M. and Cao, D.Q. (2002), “Neuro-control of cable vibration using semi-active magneto-rheological dampers”, *Eng. Struct.*, **24**(3), 295-307. https://doi.org/10.1016/S0141-0296(01)00096-7.

Or, S.W., Duan, Y.F., Ni, Y.Q., Chen, Z.H. and Lam, K.H. (2008), “Development of Magnetorheological dampers with embedded piezoelectric force sensors for structural vibration control”, *J. Intel. Mat. Syst. Str.*, **19**(11), 1327-1338. https://doi.org/10.1177/1045389X07085673.

Pasala, D.T.R., Sarlis, A.A., Reinhorn, A.M., Nagarajaiah, S., Constantinou, M.C. and Taylor, D. (2014), “Simulated bilinear-elastic behavior in asdof elastic structure using negative stiffness device: Experimental and analytical study”, *J. Struct. Eng.*, **140**(2), 04013049. https://doi.org/10.1061/(ASCE)ST.1943-541X.0000830.

Sarlis, A.A. (2013), “Negative stiffness device for seismic protection of structures”, *J. Struct. Eng.*, **139**(7), 1124-1133. https://doi.org/10.1061/(ASCE)ST.1943-541X.0000616.

Shi, X. and Zhu, S. (2015), “Magnetic negative stiffness damper and its application to stay cables”, *Proceedings of the 11th international workshop on advanced smart materials and smart structures technology*.

Smith, M.C. (2002), “Synthesis of mechanical networks: The inerter”, *IEEE T. Autom. Control*, **47**(10), 1648-1662. doi: 10.1109/TAC.2002.803532.

Smith, M.C. and Wang, F.C. (2004), “Performance benefits in passive vehicle suspensions employing inerters”, *Vehicle Syst. Dyn.*, **42**(4), 235-257. https://doi.org/10.1080/00423110412331289871.

Tabatabai, H. and Mehrabi, A.B. (2000), “Design of mechanical viscous dampers for stay cables”, *J. Bridge Eng.*, **5**(2), 114-123. https://doi.org/10.1061/(ASCE)1084-0702(2000)5:2(114).

Takewaki, I., Murakami, S., Yoshitomi, S. and Tsuji, M. (2012), “Fundamental mechanism of earthquake response reduction in building structures with inertial dampers”, *Struct. Control Health Monit.*, **19**(6), 590-608. https://doi.org/10.1002/stc.457.

Wang, F.C., Liao, M.K., Liao, B.H., Su, W.J. and Chan, H.A. (2009), “The performance improvements of train suspension systems with mechanical networks employing inerters”, *Vehicle Syst. Dyn.*, **47**(7), 805-830. https://doi.org/10.1080/00423110802385951.

Wang, X.Y., Ni, Y.Q., Ko, J.M. and Chen, Z.Q. (2005), “Optimal design of viscous dampers for multi-mode vibration control of bridge cables”, *Eng. Struct.*, **27**(5), 792-800. https://doi.org/10.1016/j.engstruct.2004.12.013.

Weber, F. and Boston, C. (2011), “Clipped viscous damping with negative stiffness for semi-active cable damping”, *Smart Mater. Struct.*, **20**(4), 13.

Weber, F., Distl, H., Feltrin, G. and Motavalli, M. (2009), “Cycle energy control of magnetorheological dampers on cables”, *Smart Mater. Struct.*, **18**(1), 16.

Weber, F., Feltrin, G., Maślanka, M., Fobo, W. and Distl, H. (2009), “Design of viscous dampers targeting multiple cable modes”, *Eng. Struct.*, **31**(31), 2797-2800. https://doi.org/10.1016/j.engstruct.2009.06.020.

Xu, Y. L. and Yu, Z. (1998), “Vibration of inclined sag cables with oil dampers in cable-stayed bridges”, *J. Bridge Eng.*, **3**(4), 194-203. https://doi.org/10.1061/(ASCE)1084-0702(1998)3:4(194).

Xu, Y.L. and Zhou, H.J. (2007), “Damping cable vibration for a cable-stayed bridge using adjustable fluid dampers”, *J. Sound Vib.*, **306**(1-2), 349-360. https://doi.org/10.1016/j.jsv.2007.05.032.

Yu, Z. and Xu, Y.L. (1998), “Mitigation of three-dimensional vibration of inclined sag cable using discrete oil dampers — i. Formulation”, *J. Sound Vib.*, **214**(4), 659-673. https://doi.org/10.1006/jsvi.1998.1609.

Zhou, P. and Li, H. (2016), “Modeling and control performance of a negative stiffness damper for suppressing stay cable vibrations”, *Struct. Control. Health Monit.*, **23**(4), 764-782. https://doi.org/10.1002/stc.1809.